University of Warsaw
Faculty of Physics

Patryk Kubiczek

Student's book no.: 322270

Geometrical model for azimuthal correlations in high-multiplicity proton-proton collisions

First cycle degree thesis
Physics, individualised studies

The thesis written under the supervision of
Prof. Stanisław Głazek
Institute of Theoretical Physics
Faculty of Physics, University of Warsaw

Warsaw, September 2014

Oświadczenie kierującego pracą

Oświadczam, że niniejsza praca została przygotowana pod moim kierunkiem i stwierdzam, że spełniła ona warunki do przedstawienia jej w postępowaniu o nadanie tytułu zawodowego.

Data Podpis kierującego pracą

Statement of the Supervisor on Submission of the Thesis

I hereby certify that the thesis submitted has been prepared under my supervision and I declare that it satisfies the requirements of submission in the proceedings for the award of a degree.

Date Signature of the Supervisor

Oświadczenie autora (autorów) pracy

Świadom odpowiedzialności prawnej oświadczam, że niniejsza praca dyplomowa została napisana przeze mnie samodzielnie i nie zawiera treści uzyskanych w sposób niezgodny z obowiązującymi przepisami.

Oświadczam również, że przedstawiona praca nie była wcześniej przedmiotem procedur związanych z uzyskaniem tytułu zawodowego w wyższej uczelni.

Oświadczam ponadto, że niniejsza wersja pracy jest identyczna z załączoną wersją elektroniczną.

Data Podpis autora (autorów) pracy

Statement of the Author(s) on Submission of the Thesis

Aware of legal liability I certify that the thesis submitted has been prepared by myself and does not include information gathered contrary to the law.

I also declare that the thesis submitted has not been the subject of proceedings resulting in the award of a university degree.

Furthermore I certify that the submitted version of the thesis is identical with its attached electronic version.

Date Signature of the Author(s) of the thesis

Summary*

Analiza korelacji wielocząstkowych w zderzeniach cząstek elemantarnych i jonów dostarcza szczegółowych informacji o mechanizmach produkcji cząstek. Nieprzewidziany przez modele teoretyczne „efekt grani” w zderzeniach proton-proton o dużej krotności jest wciąż niezrozumiany. Celem tej pracy jest zbadanie, czy zjawisko to może być wytłumaczone poprzez hydrodynamiczną ekspansję gęstej materii tworzonej w zderzeniach charakteryzujących się dużą ekscentrycznością w ramach modelu (gaussowskich) kwarków efektywnych. Wyniki obliczeń numerycznych nie dają jednoznacznej odpowiedzi.

Key words*

fizyka wysokich energii, zderzenia proton-proton, korelacje wielocząstkowe

Area of study (codes according to Erasmus Subject Area Codes List)

[13.2] Physics

The title of the thesis in Polish

Geometryczny model korelacji azymutalnych w zderzeniach proton-proton o dużej krotności

*Written in Polish

Contents

Chapter 1

Introduction

Analysis of multi-particle angular correlations in particle and ion collisions provides detailed information on the properties of particle production and allows one to reconstruct events structure in phase space. In 2010 CMS Collaboration reported on an enhanced long-range in pseudorapidity, zero-angle correlation in high-multiplicity pp collisions. This type of correlation resembles the one observed in heavy-ion collisions due to hydrodynamic expansion of colliding matter. The goal of this thesis is to verify whether the phenomenon discovered by CMS could have the same origin under several assumptions about proton internal structure and the mechanism of pp collision.

In Chapter 2 basic terms used to describe particle collisions and definition of two-particle correlations are introduced. Then, a brief overview of the ridge effect is given.

Chapter 3 discusses a possible hydrodynamic explanation of ridge-like correlation by the existence of so called elliptic flow. The hypothesis of a relation between the eccentricity of matter in the initial stage of collision and the elliptic flow in the final stage is presented.

Chapter 4 introduces the Glauber model traditionally used for modelling heavy-ion collisions and the formula for eccentricity in Glauber-described collisions.

In Chapter 5 a simple model of internal structure of proton inspired by renormalization group procedure for effective particles is proposed. In this model proton consists of three Gaussian-like effective quarks and a central Gaussian-like gluon body.

The procedure and results of Monte Carlo calculation of expected elliptic flow are the contents of Chapter 6.

The discussion of results and summary are in Chapter 7.

Chapter 2

Ridge effect

2.1. Definition of variables

Each collision of two protons is called an event. In inelastic collisions several new particles may be produced. The number of particles produced in any particular collision is called its multiplicity.

After particles produced in a collision hit detectors it is possible to determine the collision point, called the primary vertex. Then one can characterize every detected particle by providing the azimuthal angle ϕ, the polar angle θ and the value of transverse to the beam direction (z) momentum p_T (Fig. 2.1). Instead of the polar angle it is convenient to use a variable named pseudorapidity. Pseudorapidity η is defined as:

$$\eta = -\ln\left[\tan\left(\theta/2\right)\right] \tag{2.1}$$

For massless or in the limit of ultra-relativistic particles pseudorapidity coincides with rapidity $\mathrm{y} = \mathrm{artanh}(v_z/c)$ which is additive with respect to boosts along z direction. That fact makes comparison of data from different reference frames straightforward [32, 33].

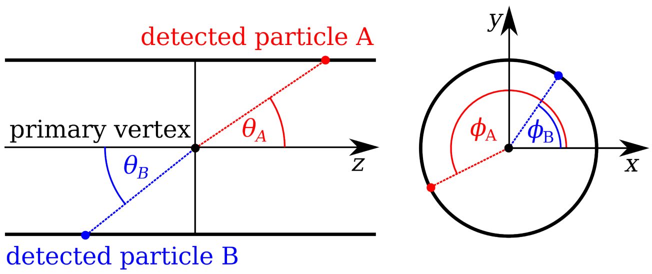

Figure 2.1: Side and front views of an event, with respect to the beam pipe. The trajectories of arbitrary two particles A and B are presented.

2.2. Two-particle correlations

In order to calculate two-particle correlations all the events are divided into several multiplicity bins. One can then determine the correlations for any single multiplicity bin or, by averaging, for all of them.

The normalized particle-pair density function S_N of relative azimuthal angle $\Delta\phi = |\phi_A - \phi_B|$ and pseudorapidity difference $\Delta\eta = |\eta_A - \eta_B|$ is constructed by combining all the pairs of produced particles at one particular event of multiplicity N belonging to a particular multiplicity bin:

$$S_N(\Delta\eta, \Delta\phi) = \frac{1}{N(N-1)} \frac{d^2 N^{\text{pairs}}}{d\Delta\eta \, d\Delta\phi} \tag{2.2}$$

The definition of two-particle correlation includes the background pair density in order to neutralize artificial correlations resulting from possible imperfections of the detectors. The background pair density function B_N is constructed by combining particles from different events belonging to the same multiplicity bin:

$$B_N(\Delta\eta, \Delta\phi) = \frac{1}{N^2} \frac{d^2 N^{\text{mixed events}}}{d\Delta\eta \, d\Delta\phi} \tag{2.3}$$

Two-particle correlation R is then defined as follows [1]:

$$R(\Delta\eta, \Delta\phi) = \left\langle (\langle N \rangle - 1) \left(\frac{S_N(\Delta\eta, \Delta\phi)}{B_N(\Delta\eta, \Delta\phi)} - 1 \right) \right\rangle_{\text{bins}}, \tag{2.4}$$

where $\langle N \rangle$ is the average multiplicity in a given bin and $\langle \ldots \rangle_{\text{bins}}$ denotes averaging over bins.

2.3. CMS data on *pp* collisions at $\sqrt{s} = 7$ TeV

The correlation function extracted from the data on charged particles produced in *pp* collisions at $\sqrt{s} = 7\,\text{TeV}$ in CERN by CMS Collaboration (Fig. 2.3) exhibits several characteristic features [1].

1. The peak at $(\Delta\eta, \Delta\phi) = (0, 0)$ is caused by jets of hadrons (Fig. 2.2). This is a consequence of the particle production mechanism in which two energetic particles of opposite momenta are produced being the sources of collimated radiation in their movement direction.

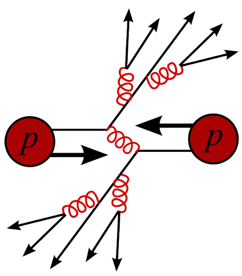

Figure 2.2: An example of two jets of collimated hadrons produced in *pp* collision

2. The elongated structure at $\Delta\phi = 2\pi$ is a signature of momentum conservation in particle production processes.

3. The new and previously not observed in *pp* collisions feature is the ridge-like structure along $\Delta\phi = 0$. This 'ridge effect' is best visible for high-multiplicity events ($N \geq 110$) in the intermediate transverse momentum range ($1\,\text{GeV}/c < p_T < 3\,\text{GeV}/c$). A similar correlation was observed in proton-lead collisions [2].

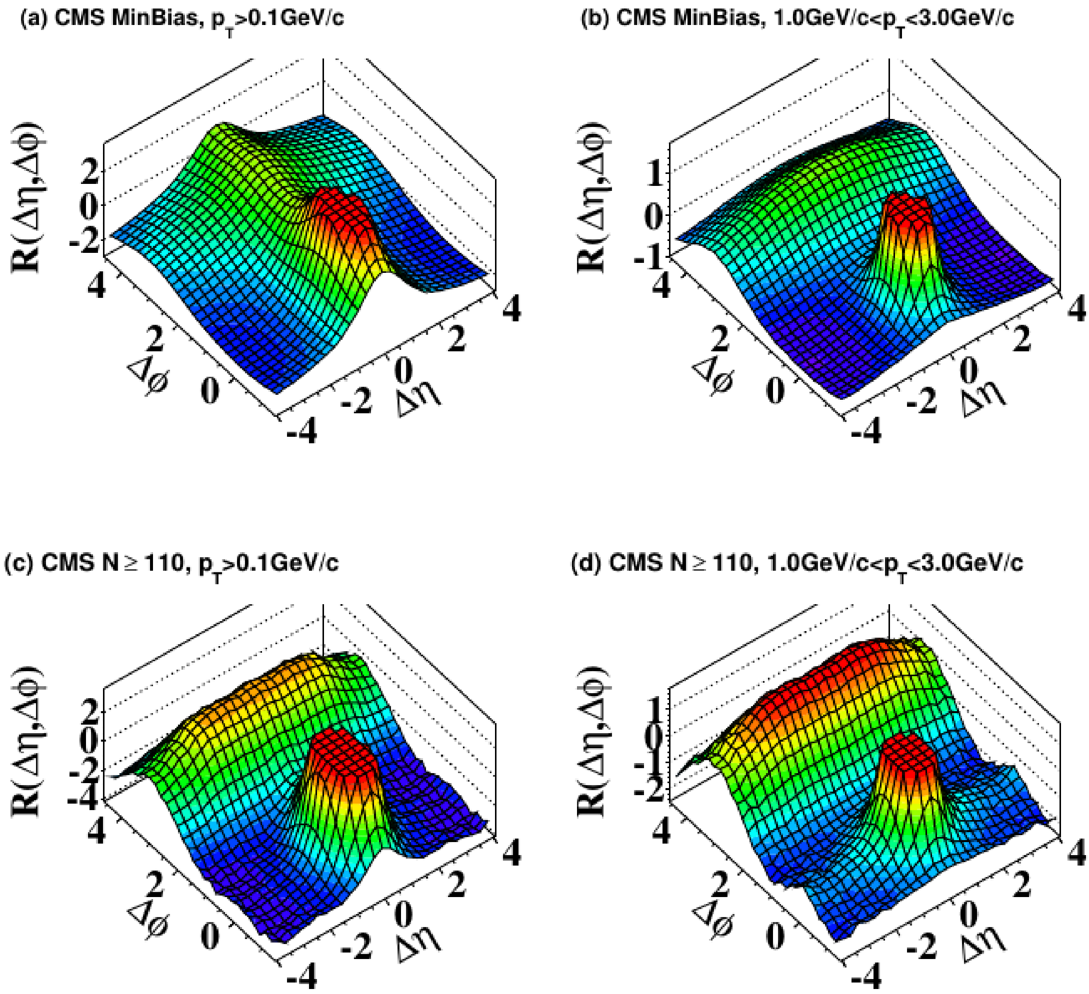

Figure 2.3: Two-particle charged hadron correlations at $\sqrt{s} = 7\,\text{TeV}$ measured by the CMS experiment: (a) for minimum bias events (averaged over all multiplicities), (b) for minimum bias events and the intermediate transverse momentum range, (c) for high-multiplicity events, (d) for high-multiplicity events and the intermediate transverse momentum range [1]

2.4. Possible ridge effect explanations

There is no obvious reason why such a long-range in pseudorapidity correlation should occur. There are many theoretical interpretations of the phenomenon which in general belong to one of the two categories of initial or final state effects [3, 4, 5, 6].

It is possible to explain the ridge effect by the initial state dynamics in the framework of the *color glass condensate* effective theory [7]. The ridge structure in that case would originate from the ladder diagrams contribution to the gluonic interactions, which is non-negligible in case of gluon saturation expected to take place in high-multiplicity events.

The other type of possible explanation is based on the assumption of multiple interactions of produced particles in the collision final state. The ridge-like correlation in that case originates from the elliptic component of the expanding matter collective flow. This effect was previously observed in heavy-ion collisions and was well described hydrodynamically. Such an idea is presented e.g. by [8, 9, 10]. The more detailed discussion of this explanation, being the working hypothesis of this thesis, is presented in Chapter 3.

This brief review is by no means complete as the number of theoretical models for the ridge effect is large. At the moment the data from CMS seems not to be precise enough to distinguish between them as the most are able to explain the phenomenon. Thus, according to [6] high-multiplicity pp collisions can be regarded now as *Pandora's box* hiding information that could possibly lead to new insights on hadron structure.

Chapter 3

Hydrodynamic description

3.1. Elliptic flow

Ridge effect has been observed in relativistic heavy-ion collisions. The plausible explanation was the collective flow of hot and dense medium created during a collision and having an initial spatial anisotropy. The observation of elliptic flow in heavy-ion collisions is considered an evidence that this medium is a quark-gluon plasma behaving like a strongly coupled liquid with small viscosity [33].

The interaction volume of two ions can be anisotropic in xy plane for two reasons: a non-zero impact parameter b (Fig. 3.1) and an event-by-event fluctuating, non-uniform distribution of the nucleons in the colliding nuclei. If a hydrodynamical evolution of this medium is assumed, the initial spatial anisotropy is transferred by pressure gradient into the similar anisotropy in final momenta. The azimuthal angle anisotropy in single-particle momentum yield can be decomposed into Fourier series [11]:

$$\frac{d^3N}{d^2p_\mathrm{T}d\eta} = \frac{d^2N}{2\pi p_\mathrm{T}dp_\mathrm{T}d\eta}\left(1+2\sum_{n=1}^{\infty}v_n(p_\mathrm{T},\eta)\cos\left[n(\phi-\Phi_\mathrm{RP})\right]\right) \tag{3.1}$$

where $v_n(p_\mathrm{T},\eta) = \langle\cos\left[n(\phi-\Phi_\mathrm{RP})\right]\rangle$. The second coefficient v_2 is called elliptic flow coefficient. The reaction plane angle Φ_RP defines a long and a short axis of the elliptical shape of the initial spatial distribution. When one takes into account fluctuations of nucleons' positions a participant plane angle Φ_PP must replace Φ_RP and they do not need to coincide with each other. The methods for determining Φ_RP and Φ_PP are presented in [33].

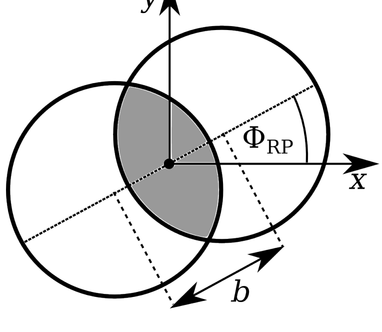

Figure 3.1: Elliptic shape of interacting matter. For isotropic densities of ions $\Phi_\mathrm{RP} = \Phi_\mathrm{PP}$.

There is a crucial relation between v_n and two-particle azimuthal correlation [11]:

$$\langle \cos(n\Delta\phi) \rangle = \left\langle e^{in\Delta\phi} \right\rangle = \left\langle e^{in(\phi_{\mathrm{A}}-\Phi_{\mathrm{RP}})} e^{-in(\phi_{\mathrm{B}}-\Phi_{\mathrm{RP}})} \right\rangle = v_n^2 + \delta_n \tag{3.2}$$

where $\Delta\phi = \phi_A - \phi_B$ is the difference between particle A and B azimuthal angles and δ_n is a non-flow correlation. Here a negligibility of δ_2 is assumed. A non-zero v_2 would manifest itself in two-particle correlation in a form of ridges in $\Delta\phi = 0$ and $\Delta\phi = \pi$ as $\cos(2\Delta\phi)$ is positive in these regions. Such ridges are present in the CMS data (Fig. 2.3) and assuming the existence of elliptic flow it is possible to extract from it η-integrated v_2 coefficients for different p_T. Such analysis was done by Bożek [9] and its results are presented in Fig. 3.2. However, the elliptic flow correlations are subleading and the necessity to propose a model for the dominant effects makes such procedure unambiguous

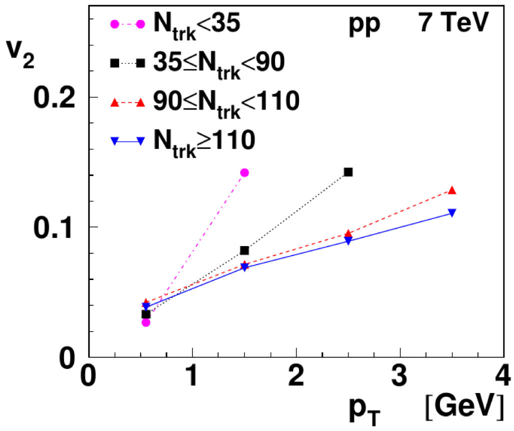

Figure 3.2: Elliptic flow $v_2(p_{\mathrm{T}})$ for the four multiplicity classes extracted from the CMS data [9]

3.2. Relation between elliptic flow and initial eccentricity

It is very appealing to assume that there is some relationship between the initial spatial anisotropy of colliding matter called eccentricity and the final momentum anisotropy being the elliptic flow. The eccentricity is ϵ defined as:

$$\epsilon = \frac{\sigma_{y'}^2 - \sigma_{x'}^2}{\sigma_{y'}^2 - \sigma_{x'}^2}, \tag{3.3}$$

where

$$\sigma_{x'}^2 = \left\langle x'^2 \right\rangle - \left\langle x' \right\rangle^2$$
$$\sigma_{y'}^2 = \left\langle y'^2 \right\rangle - \left\langle y' \right\rangle^2$$

and x', y' are x, y rotated by angle Φ_{RP} (or Φ_{PP}) such that x' and y' always correspond respectively to the short and the long axis of the elliptical shape (Fig. 3.1).

The result of the hydrodynamic calculations in [12] is that the p_T- and η-integrated v_2 as a function of the mean value of ϵ may be roughly approximated by the formula:

$$\frac{v_2}{\epsilon} = \left(\frac{v_2}{\epsilon}\right)^{\mathrm{hydro}} \frac{1}{1 + K/K_0} \tag{3.4}$$

where $(v_2/\epsilon)^{\mathrm{hydro}} = 0.3$, the ideal hydrodynamics limit value, and $K_0 = 0.7$. Knudsen number $K = \lambda/R$ is a ratio of mean free path λ of partons constituting the medium to the transverse size R of the medium. Non zero K corresponds to the case of not completely thermalized system, while in the limit of high density of partons and high partonic cross section when $K = 0$ the ideal hydrodynamic limit is obtained. Knudsen number is approximated by the formula:

$$K = \frac{S}{\sigma_{\mathrm{gg}}\, c_s\, \frac{dN}{dy}}, \tag{3.5}$$

where $\sigma_{\mathrm{gg}} = 4.3$ mb is a cross section for parton-parton interaction, $c_s = 1/\sqrt{3}$ is a theoretical speed of sound in partonic medium, dN/dy is produced particle multiplicity at zero rapidity and S is a mean transverse size of the system:

$$S = 4\pi\sigma_{x'}\sigma_{y'} \tag{3.6}$$

All the numbers provided above reproduce well the data on heavy-ion collisions with Glauber initial conditions (Chapter 4).

It is not known whether quark-gluon plasma can be produced in pp collisions or whether hydrodynamics is applicable in such small systems. Nevertheless, the goal of the thesis is to build a model for the eccentricity ϵ and compare v_2 it implies according to (3.4) with v_2 extracted from the data.

What is worth noticing is that the eccentricity in pp collisions can be generated in two ways. Besides the obvious one due to non-zero impact parameter there can also be anisotropy generated by non-trivial internal proton's structure. In that case one needs to determine the participant plane angle Φ_{PP} in each event. However, this step can be omitted by use of an improved definition of eccentricity. The detailed discussion of such a calculation of the eccentricity is the topic of Chapter 4.

Chapter 4

Estimation of colliding matter eccentricity

4.1. Glauber model

There exists a standard technique for describing the geometry of heavy-ion collisions. The analogous technique is used in this thesis for pp collisions, the essence of the analogy being the correspondence of nuclei and nucleons respectively with protons and partons constituting proton.

The aforementioned technique is based on the Glauber model. The original quantum-mechanical model was proposed by Glauber in 1958 [13]. It enabled one to calculate the phase shifts in scattering of ions. The Glauber treats the collision of two composite nuclei (protons) as a superposition of collisions of the nucleons (partons) they are made of. Its main assumptions are:

- the interaction between the constituent particles during the collision is negligible,
- the constituents move along straight lines during the collision,
- the scattering is mostly in the forward direction.

In this thesis the classical limit of the Glauber model is used in order to estimate the eccentricity of colliding matter. This simplified model, known as wounded nucleons model, was introduced by Białas, Błeszyński and Czyż in 1976 [14].

The input information to the wounded nucleon model are the positions of nucleons in the nuclei and nucleon-nucleon cross sections. The output is the inelastic nucleus-nucleus cross section and the number density of nucleon-nucleon collisions. These collisions are assumed to be the source of particles forming the matter which is evolving hydrodynamically in the later part of collision. It is the collision density that is used to estimate the density of interaction volume which allows one to calculate its geometrical quantities [15].

The first step of the Glauber model is to project the density of constituent matter $\rho(x, y, z)$ normalized to the mass number N_A onto the plane perpendicular to the beam direction:

$$T_A(x, y) = \int_{-\infty}^{\infty} \rho(x, y, z) dz \tag{4.1}$$

The density of nucleon-nucleon collisions is then given by the formula:

$$n_{\text{coll}}(x, y; b) = \sigma_{NN}\, T_A(x - \frac{b}{2}, y)\, T_B(x + \frac{b}{2}, y), \tag{4.2}$$

where σ_{NN} is a nucleon-nucleon cross section and b is the impact parameter vector.

In order to obtain the total number of nucleon-nucleon collisions one needs to integrate the above formula:

$$N_{\text{coll}}(b) = \sigma_{NN} \int dx\, dy\, T_A(x - \frac{b}{2}, y)\, T_B(x + \frac{b}{2}, y) \tag{4.3}$$

Glauber model is used to describe produced particle multiplicities in heavy-ion collisions. One postulates that the multiplicity per impact parameter $N(b)$ is proportional to the number of binary collisions or to the number of wounded nucleons (i.e. the ones which collided with at least one nucleon from the other nucleus).

The leading mechanism for particle production in pp collisions are mini-jets caused by partonic interactions so it is postulated in this thesis that the number of produced particles scales with the number of parton-parton collisions:

$$N(b) = \alpha N_{\text{coll}}(b) \tag{4.4}$$

If the mean multiplicity of collisions is measured and the mean number of binary collisions is calculated the proportionality constant α can be determined.

The differential inelastic cross section may be expressed as [15, 33]:

$$\frac{d\sigma}{db} = 2\pi b \left[1 - \left(1 - \frac{N_{\text{coll}}(b)}{N_A N_B} \right)^{N_A N_B} \right] \tag{4.5}$$

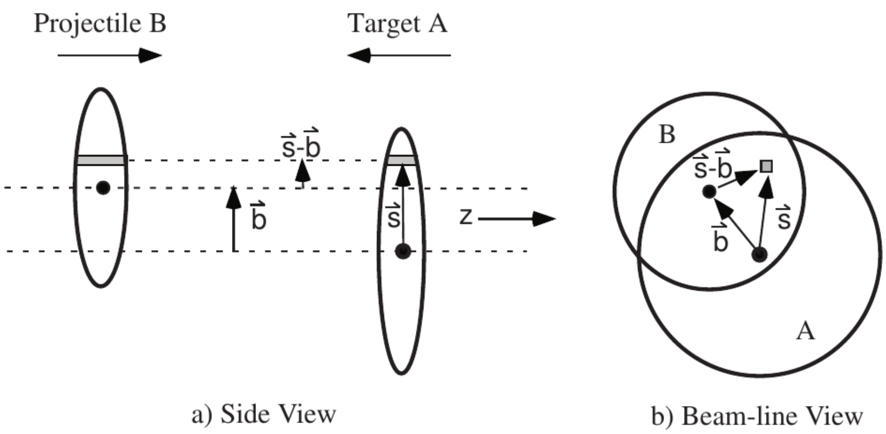

Figure 4.1: Side and beam-line view of colliding particles ($\mathbf{s} = (x, y)$) [15]

4.2. Eccentricity calculation

The basic definition of eccentricity was already introduced by (3.3). That definition is useful if the short and the long axis of the elliptic shape (x' and y') are known. It is reasonable that for an arbitrary matter distribution they should maximize the value of σ'_y and minimize σ'_x. Eccentricity obtained in this way is called participant eccentricity and is given by formula (4.6) for any choice of x and y [16]. From now on it will serve as the definition of eccentricity:

$$\epsilon = \frac{\sqrt{\left(\sigma_y^2 - \sigma_x^2\right)^2 + 4\sigma_{xy}^2}}{\sigma_y^2 + \sigma_x^2}, \tag{4.6}$$

where

$$\begin{aligned} \sigma_x^2 &= \left\langle x^2 \right\rangle - \langle x \rangle^2 \\ \sigma_y^2 &= \left\langle y^2 \right\rangle - \langle y \rangle^2 \\ \sigma_{xy}^2 &= \langle xy \rangle - \langle x \rangle \langle y \rangle \end{aligned}$$

and the average values are weighted by the density of nucleon-nucleon collisions $n_{coll}(x, y; \mathbf{b})$. Similarly, the transverse area of interaction introduced by (3.6) can now be calculated by the formula:

$$S = 4\pi\sqrt{\sigma_x^2\sigma_y^2 - \sigma_{xy}^2} \tag{4.7}$$

One needs to perform a calculation of the eccentricity and transverse size for each event separately.

Chapter 5

Model of proton's internal structure

5.1. Concept of effective quarks

There are two distinct pictures of proton's internal structure: 1) proton built from three "constituent" quarks and 2) proton containing point-like partons: "current" quarks and gluons. The first picture arises from its ability to account for hadronic spectra, while the second explains well the results of hard scattering experiments. Renormalization group procedure for effective particles (RGPEP) offers a bridge between these points of view suggesting that the effective size of constituent quark can strongly depend on the energy scale used to probe proton [17]. The larger the momentum transfer Q in partonic collisions, the smaller particles are required for a simple description of observables. For $Q = \Lambda_{\mathrm{QCD}}$, the characteristic energy for strong interactions, quarks can even be as big as whole proton (Fig. 5.1). One should note that the overlap of big quarks makes proton white and in case of smaller quarks locally white gluon medium (gluons and the sea of quark-antiquark pairs) fills proton in.

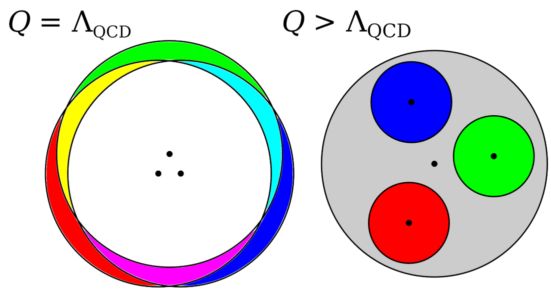

Figure 5.1: RGPEP picture of proton at energy scale $Q = \Lambda_{\mathrm{QCD}}$ and $Q > \Lambda_{\mathrm{QCD}}$ [17].

5.2. Model of proton's density profile

In this thesis a simple model of proton inspired by the effective quark picture is analyzed. Proton is assumed to consist of three effective quarks, homogeneously charged two ups ($+2/3\ e$) and one down (-1/3 e), and a gluon body of certain radii. The effective quarks and the gluon body are clusters of partons which is in resemblance with known two stage models [18, 19, 20] used to explain the shape of deep inelastic scattering structure functions.

The parameters of the model are:

- N_g - the total number of partons in a proton,
- κ - the ratio of the number of partons in the gluon body to N_g
- r_q - radius of the effective quark,
- r_g - radius of the gluon body,
- R_P - radius characterizing effective quarks' distribution in proton.

The partons' number densities (parton densities) of the effective quark and the gluon body are assumed to be 3D isotropic Gaussian functions:

$$\rho_q(r) = (1-\kappa)\frac{N_g}{3}\frac{1}{(2\pi)^{3/2}\, r_q^3} e^{-r^2/2r_q^2} \tag{5.1}$$

$$\rho_g(r) = \kappa N_g \frac{1}{(2\pi)^{3/2}\, r_g^3} e^{-r^2/2r_g^2} \tag{5.2}$$

One can see from (5.1) that each effective quark is expected to carry the same number of partons.

The root-mean-square value of the Gaussian distribution is equal to its variance times $\sqrt{3}$. Quark radius r_q should than be compared to the proton radius r_p in the same parametrization. The rms charge radius of proton $R_{\text{rms}} = 0.88\,\text{fm}$ is known from experiment, thus:

$$r_p = \frac{R_{\text{rms}}}{\sqrt{3}} \approx 0.5\,\text{fm}, \tag{5.3}$$

RGPEP suggests that when quark radii correspond to the proton radius then no central gluon body is needed to describe proton. A simple formula for κ being in agreement with this observation which will be used for calculations is:

$$\kappa = 1 - \frac{r_q}{r_p} \tag{5.4}$$

In the center of mass frame the parton density of the proton is given at point $\mathbf{r}$ by the expression

$$\rho_p(\mathbf{r}; \mathbf{r}_1, \mathbf{r}_2, \mathbf{r}_3) = \sum_{i=1}^{3} \rho_q(\mathbf{r} - \mathbf{r}_i) + \rho_g(\mathbf{r}), \tag{5.5}$$

where $\mathbf{r}_1, \mathbf{r}_2, \mathbf{r}_3$ are some positions of three effective quarks fixed during a collision satisfying the relation:

$$\mathbf{r}_1 + \mathbf{r}_2 + \mathbf{r}_3 = 0 \tag{5.6}$$

For simplicity the Gaussian probability distribution of the effective quarks' positions is used:

$$P(r_1, r_2, r_3) = \frac{1}{[(2\pi)^{3/2}\, R_P^3]^3} e^{-(r_1^2+r_2^2+r_3^2)/2R_P^2}, \tag{5.7}$$

where $r_i = |\mathbf{r}_i|$. It is reasonable to assume that the radius r_g of gluon body which is responsible for binding quarks is no smaller than the radius of quarks' distribution R_P. Hereafter, the equality of them is assumed.

The model should reproduce the known rms charge radius of proton which is the average of many measurements. When the proton density is averaged over effective quarks' positions with the Gaussian distribution (5.7) the following constraint is obtained:

$$r_p^2 = R_P^2 + r_q^2 \tag{5.8}$$

No effective quarks larger than the proton itself can be considered in this model.

One should note that the use of Gaussian functions greatly simplifies all the necessary integration over z as the integral of the 3D Gaussian over one of its variables is 2D Gaussian.

Chapter 6

Monte Carlo simulation

6.1. Procedure

Each collision of protons within the model introduced in Chapter 5 is characterized not only by impact parameter but also by the positions of six effective quarks. In consequence, when calculating expected values of quantities characterizing pp collisions one needs to average over the space of all the possible configurations of two protons. For each impact parameter b the following procedure was carried on:

1. Proton thickness function (4.1) is calculated by integrating (5.5) over variable z.
2. Thickness function does not depend on z-components of effective quarks positions so the distribution of quarks in proton (5.7) is z-integrated.
3. According to the probability distribution from step 2, x and y coordinates for each of 3 quarks in proton A are generated (6 numbers at total). The generated configuration has to satisfy the center-of-mass relation (5.6) so each of the quark 2D position is shifted by a vector $-(\mathbf{s}_1^A + \mathbf{s}_2^A + \mathbf{s}_3^A)/3$.*
4. Step 3 is repeated for proton B.
5. The collision density is now determined according to (4.2) with the protons' densities being separated by the impact parameter b along x-axis (Fig. 6.1). Instead of nucleon-nucleon cross section σ_{NN}, parton-parton cross section σ_{gg} is used.

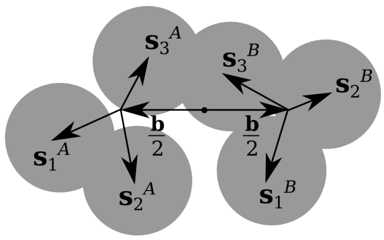

Figure 6.1: 2D projection of a sample event

6. An eccentricity and other quantities of the given configuration are calculated.

*Vector $\mathbf{s}_i^j$ consists of x and y coordinates of ith quark in jth proton ($i = 1, 2, 3$, $j = A, B$).

7. The steps 3-6 are repeated sufficiently many times to estimate the mean values of interest. The number of necessary iterations was determined by demanding that the results fluctuate no more than 1% in consequent calculations.

One of the outputs of the procedure described above is the inelastic pp cross section calculated within the Glauber model by integrating (4.5) (with proton configuration $\mathbf{\Sigma} = (\mathbf{s}_1^A, \mathbf{s}_2^A, \mathbf{s}_3^A, \mathbf{s}_1^B, \mathbf{s}_2^B, \mathbf{s}_3^B)$ dependence added) over all impact parameters and quarks' positions:

$$\sigma_{pp} = \int \cdots \int \int_0^\infty \frac{d\sigma_{pp}}{db}(b, \mathbf{\Sigma})\, db\, d^{12}\Sigma, \tag{6.1}$$

where

$$d^{12}\Sigma = P(s_1^A, s_2^A, s_3^A)\, P(s_1^B, s_2^B, s_3^B) \prod_{i=1}^{3} d^2 s_i^A \prod_{i=1}^{3} d^2 s_i^B \tag{6.2}$$

and $P(s_1, s_2, s_3)$ is the 2D probability distribution obtained by integrating (5.7) in step 2. The integration over $\mathbf{\Sigma}$ is being done by means of Monte Carlo sampling. It is not possible to solve it analytically because $\frac{d\sigma_{pp}}{db}$ depends on $\mathbf{\Sigma}$ only through N_{coll} which is given by a non-trivial expression. All the relative positions of the effective quarks have to be taken into account so the integral dimension cannot be reduced.

The first step was to determine N_g by the demand of reproducing the experimentally known inelastic cross section of 60 mb for $\sqrt{s} = 7\,\mathrm{TeV}$ [21]. The parton-parton cross section σ_{gg} was assumed to be 4.3 mb, the same value as in (3.5). For each set of parameters the bisection method was used in order to return the value of N_g. In each step of the bisection σ_{pp} as a function of N_g was calculated with 30 000 Monte Carlo iterations. The bisection procedure terminated when σ_{pp} equalled 60 mb with 1% accuracy.

In the second step the mean number of collisions in an event $\langle N_{coll} \rangle$ was calculated with 30 000 Monte Carlo samples:

$$\langle N_{coll} \rangle = \frac{1}{\sigma_{pp}} \int \cdots \int \int_0^\infty N_{coll}(b, \mathbf{\Sigma})\, \frac{d\sigma_{pp}}{db}(b, \mathbf{\Sigma})\, db\, d^{12}\Sigma \tag{6.3}$$

Knowing that the minimum bias inelastic multiplicity for $\sqrt{s} = 7\,\mathrm{TeV}$ is 30 [22] the constant α from (4.4) could be determined. The constant α is assumed to represent a number of particles produced in one parton-parton collision. The differential multiplicity at zero rapidity dN/dy was approximated in the same way:

$$\frac{dN}{dy}(b, \mathbf{\Sigma}) = \gamma N_{coll}(b, \mathbf{\Sigma}), \tag{6.4}$$

the constant γ determined by demanding that mean dN/dy is 5.8 [23].

The final step was to perform much more accurate Monte Carlo sampling in order to calculate the expected elliptic flow coefficient. For each of 600 000 proton configuration samples the eccentricity (4.6), mean transverse size (3.6), multiplicity at midrapidity (6.4) and eventually v_2 (3.4) were calculated.

It is v_2^2, not v_2, that is extracted from two-particle correlation (3.2). Thus, in order to compare it with the result of calculations, one should determine the expected value of v_2^2 and then take a square root of it. There is no ambiguity about the sign of v_2 as it is always assumed to be positive according to (3.4). It is also necessary to multiply each v_2^2 by a weighting factor of multiplicity $N = \alpha N_{coll}$ (factor α drops out in the below equation) in a given event as the correlation function presented by CMS is the average of correlations in bins multiplied by the average bin multiplicity [1]:

$$\langle v_2^2 \rangle = \frac{1}{\langle N_{coll} \rangle \, \sigma_{pp}} \int \cdots \int \int_0^\infty v_2^2(b, \mathbf{\Sigma}) N_{coll}(b, \mathbf{\Sigma}) \, \frac{d\sigma_{pp}}{db}(b, \mathbf{\Sigma}) \, db \, d^{12}\Sigma \tag{6.5}$$

In addition to performing calculations on minimum-bias events, elliptic flow and other interesting quantities were calculated also only for high-multiplicity events. The trigger for classifying an event to this category (set by the author of the thesis) was the multiplicity approximated by (4.4) higher than 85 particles. Such events constitute (0.1 - 3)% of all the events (depending on parameters r_q and κ) which is of the same order of magnitude as the percentage of $N > 110$ CMS events (1.6%).

6.2. Results

The most important results were the values of elliptic flow coefficient, which can be compared to [9], and the shapes of multiplicity distributions, compared to the experimentally measured [22, 23]. The differential cross section mean number of binary collisions and mean eccentricity per b were calculated to present a structure of the event in the impact parameter space. The eccentricity distributions in events were also determined to assess the range of occurring eccentricities.

The results of calculations for several values of quark radius when κ follows the dependence (5.4) are presented in Table 6.1. Only radii larger than $r_p/2 = 0.25$ fm were considered. The expected v_2 for minimum bias (MB) events lies in the range of 0.02 - 0.04 while for high-multiplicity events (HM) it is not significantly different. The ridge in the two-particle correlation is proportional to v_2^2 times the mean multiplicity in a bin [9]. The non-flow correlations ignored in the calculations is probably the reason why the ridge can be distinguished from the background only in the highest multiplicity bin.

The multiplicity distributions, based on the number of produced particles to number of collisions proportionality, are shown in Fig. 6.2. They do not reproduce well experimental hadron multiplicity distribution which exhibits much longer tail of high-multiplicity events [22].

Differential cross section (Fig. 6.6) and the mean number of partonic collisions as a function of b (Fig. 6.4) do not exhibit considerable dependence on r_q nor κ and that is why the plots of these quantities are presented only for the case $\kappa = 1 - r_q/r_p$. The area under the plot of differential cross section always equals the total (inelastic) cross section of 60 mb. The mean number of binary collisions decreases with b very strongly which is observed for other parametrizations of proton density as well [26].

Unweighed event eccentricity distributions (Fig. 6.5) have a maximum around $\epsilon = 0.1$ and are getting more and more wide with decreasing r_q. The reason for this is the widening with r_q distribution of quark positions due to (5.7) which makes chances for eccentric configurations higher.

Remarkably, for medium r_q the mean eccentricity is always highest in central collisions (Fig. 6.6) contrary to the expectation that it would be highest for medium values of b by when the overlapping densities have almond-like shape (Fig. 3.1). However, one should remember that it is fluctuating quark configuration and not smooth isotropic density of proton considered here.

The results of calculations in the limit $r_q = r_p$ are shown in Table 6.2 and Fig. 6.7. In this limiting case the fluctuations of quarks positions are frozen and the parametrization of proton is one Gaussian function. The product of two isotropic Gaussian functions is isotropic even if the origins do not coincide. Therefore, there can be no eccentricity. This would be unrealistic in heavy-ion collisions where the eccentricity due to the non-zero impact parameter is believed to occur. However, it may be that the main source of the eccentricity in pp collisions are fluctuating quark configurations.

The central gluon body influence on the results was analyzed by loosening the constraint (5.4) and performing calculations for three chosen constant values of κ: 0, 0.25, 0.5.

The results for $\kappa = 0$ corresponding to the case without the gluon body are presented in Table 6.3. The expected v_2 can be as high as 0.07 - 0.08 for $r_q = 0.25$ fm. The multiplicity distributions (Fig. 6.8) for medium quark radii cover a very broad range, similar to the one observed experimentally. It can be easily understood as high density configurations of overlapping quarks are more probable since the whole mass of proton is contained in quarks. The eccentricity distributions (Fig. 6.9) are also much wider and mean eccentricities (Fig. 6.10) reach relatively high values.

An interesting feature is seen for $\kappa = 0.25$ and 0.5. A huge eccentricity occurs in mid-central collisions for large quark radii (Fig. 6.13, 6.16). It resembles the one due to the almond-like shape of collision region (Fig. 3.1). However, it turns out the source of the anisotropy is an elongation of collision density along the impact parameter vector (90-degree rotated almond shape). The illustration is provided in Fig. 6.17. The eccentricity obtained in this way would imply a strong ridge effect in the medium multiplicity bins, which consist of the mid-central collisions according to the Glauber model. For this reason, the set of parameters leading to this effect should be disregarded.

Table 6.1: Results for minimum bias and high-multiplicity (HM) events

Input					
Quark radius r_q [fm]	0.25	0.30	0.35	0.40	0.45
Gluon body content κ	0.5	0.4	0.3	0.2	0.1
Effective partonic cross section σ_{gg} [mb]	4.3	4.3	4.3	4.3	4.3
Output					
Effective number of partons N_g	6.4	6.5	6.5	6.1	5.7
Mean number of parton collisions $\langle N_{\text{coll}} \rangle$	2.5	2.7	2.7	2.3	1.9
Produced particles parton collision α	11.8	11.1	11.3	13.2	16.1
dN/dy per parton collision γ	2.3	2.1	2.2	2.6	3.1
Mean eccentricity $\langle \epsilon \rangle$	0.18	0.18	0.17	0.13	0.09
RMS eccentricity $\sqrt{\langle \epsilon^2 \rangle}$	0.22	0.21	0.20	0.16	0.10
Mean eccentricity in HM events $\langle \epsilon \rangle_{\text{HM}}$	0.18	0.15	0.13	0.09	0.05
RMS eccentricity in HM events $\sqrt{\langle \epsilon^2 \rangle_{\text{HM}}}$	0.20	0.17	0.14	0.10	0.05
Expected elliptic flow $\sqrt{\langle v_2^2 \rangle}$	0.04	0.04	0.03	0.03	0.02
Expected elliptic flow in HM events $\sqrt{\langle v_2^2 \rangle_{\text{HM}}}$	0.05	0.04	0.03	0.02	0.01
Fraction of HM events	0.03	0.03	0.03	0.03	0.01

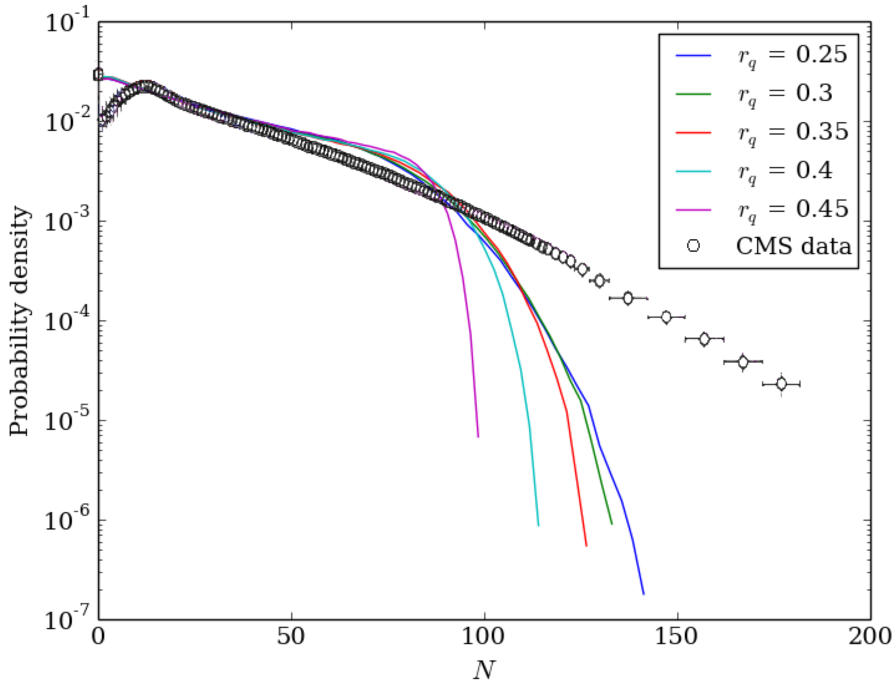

Figure 6.2: Event multiplicity distribution for $\kappa = 1 - r_q/r_p$ compared with [22]

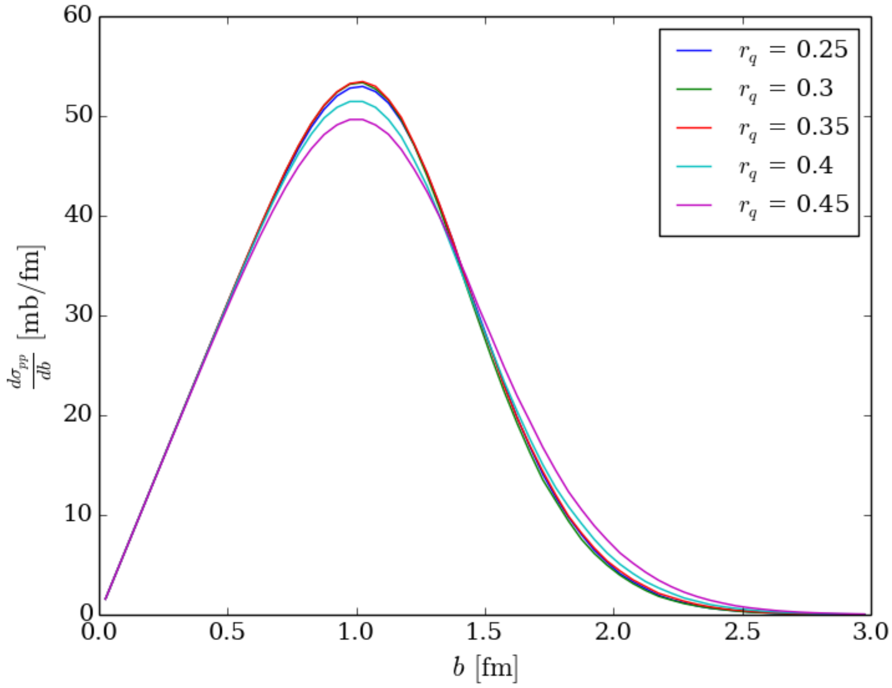

Figure 6.3: Differential cross section as a function of impact parameter b for $\kappa = 1 - r_q/r_p$

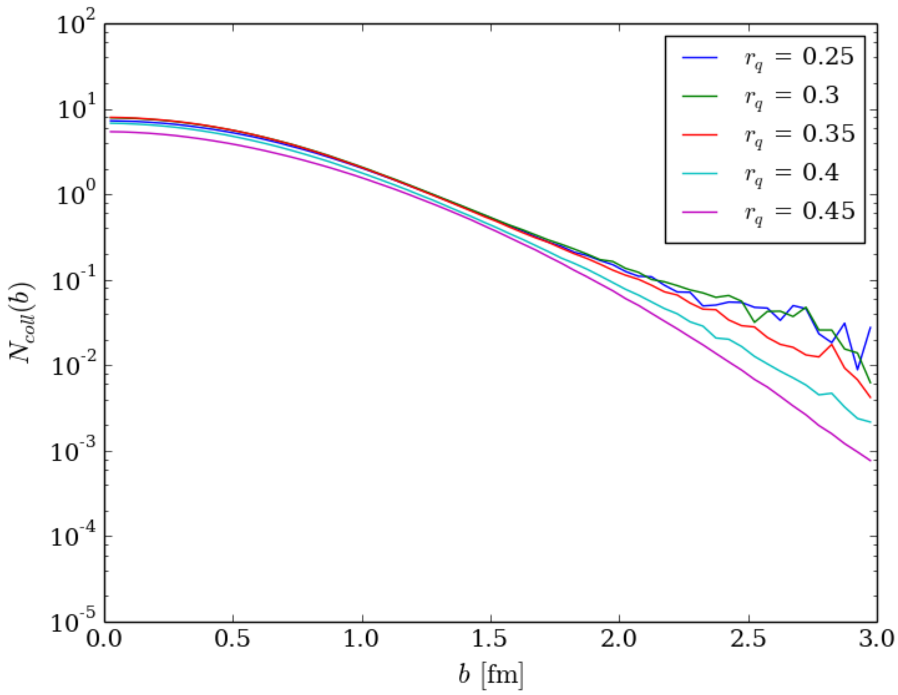

Figure 6.4: Mean number of binary partonic collisions as a function of impact parameter b for $\kappa = 1 - r_q/r_p$

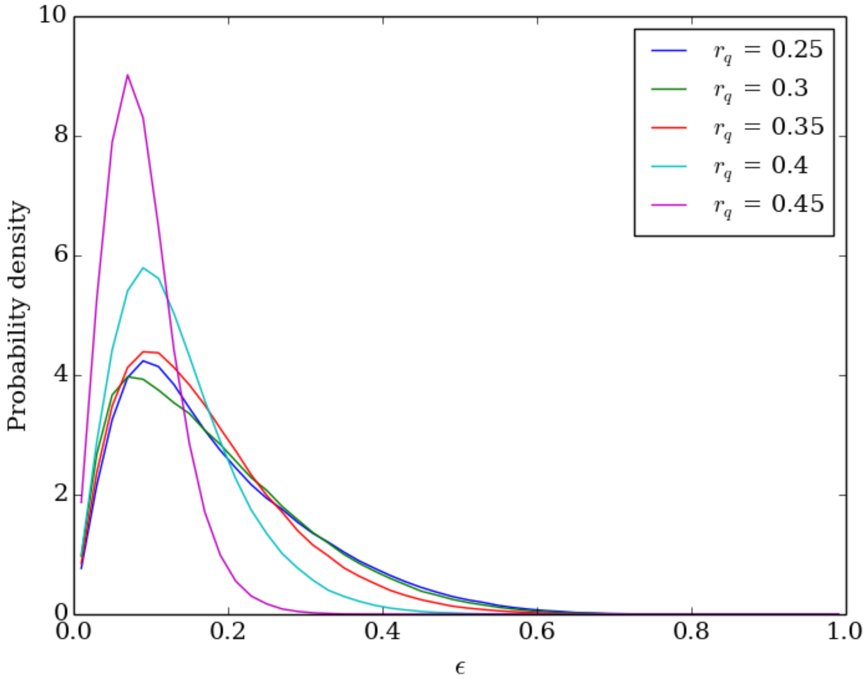

Figure 6.5: Event eccentricity distribution for $\kappa = 1 - r_q/r_p$

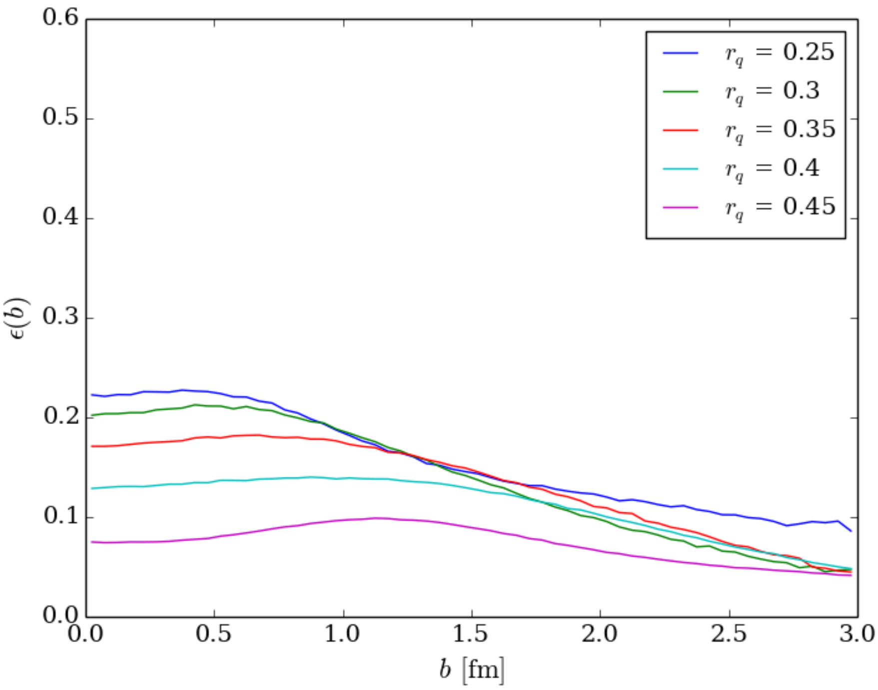

Figure 6.6: Mean eccentricity as a function of impact parameter b for $\kappa = 1 - r_q/r_p$

Table 6.2: Results for minimum bias events for one Gaussian parametrization of proton's density

Input	
Quark radius r_q [fm]	0.5
Gluon body content κ	any
Effective partonic cross section σ_{gg} [mb]	4.3
Output	
Effective number of partons N_g	5.2
Mean number of parton collisions $\langle N_{\text{coll}} \rangle$	1.4
Produced particles per parton collision α	20.9
dN/dy per parton collision γ	4.0
Mean eccentricity $\langle \epsilon \rangle$	0
Expected elliptic flow $\sqrt{\langle v_2^2 \rangle}$	0

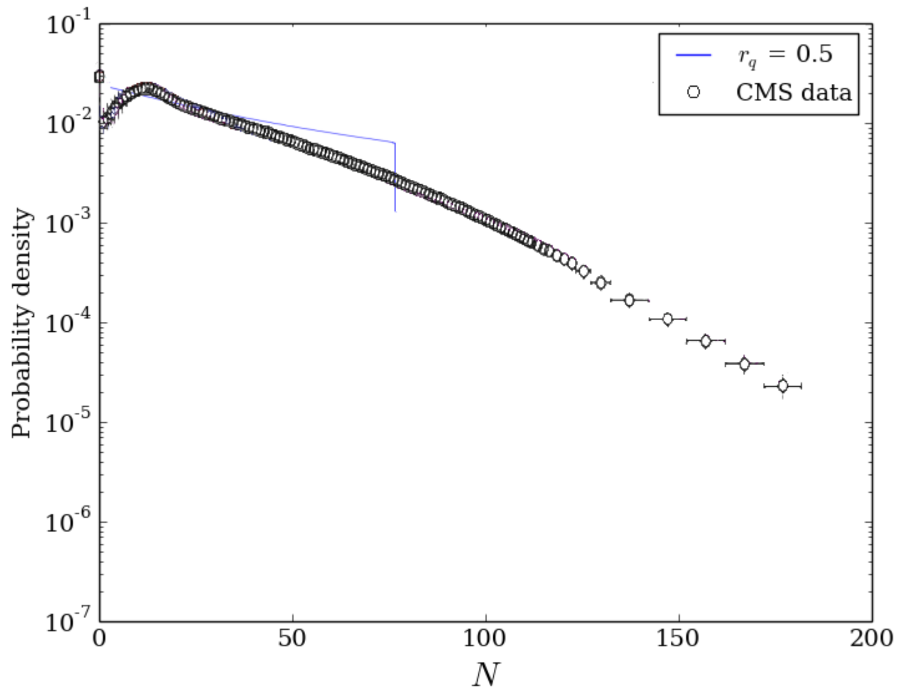

Figure 6.7: Event multiplicity distribution for one Gaussian parametrization of proton's density compared with [22]

Table 6.3: Results for minimum bias and high-multiplicity (HM) events without central gluon body ($\kappa = 0$)

Input					
Quark radius r_q [fm]	0.25	0.30	0.35	0.40	0.45
Gluon body content κ	0	0	0	0	0
Effective partonic cross section σ_{gg} [mb]	4.3	4.3	4.3	4.3	4.3
Output					
Effective number of partons N_g	7.6	6.6	6.0	5.6	5.4
Mean number of parton collisions $\langle N_{\text{coll}} \rangle$	3.9	2.8	2.1	1.8	1.6
Produced particles per parton collision α	7.7	11.0	14.0	16.2	18.6
dN/dy per parton collision γ	1.5	2.1	2.7	3.1	3.6
Mean eccentricity $\langle \epsilon \rangle$	0.28	0.25	0.20	0.13	0.07
RMS eccentricity $\sqrt{\langle \epsilon^2 \rangle}$	0.35	0.30	0.24	0.16	0.09
Mean eccentricity in HM events $\langle \epsilon \rangle_{\text{HM}}$	0.30	0.22	0.15	0.09	0.03
RMS eccentricity in HM events $\sqrt{\langle \epsilon^2 \rangle_{\text{HM}}}$	0.34	0.26	0.17	0.10	0.03
Expected elliptic flow $\sqrt{\langle v_2^2 \rangle}$	0.07	0.05	0.04	0.03	0.01
Expected elliptic flow in HM events $\sqrt{\langle v_2^2 \rangle_{\text{HM}}}$	0.08	0.06	0.04	0.02	0.01
Fraction of HM events	0.04	0.03	0.02	0.01	0.001

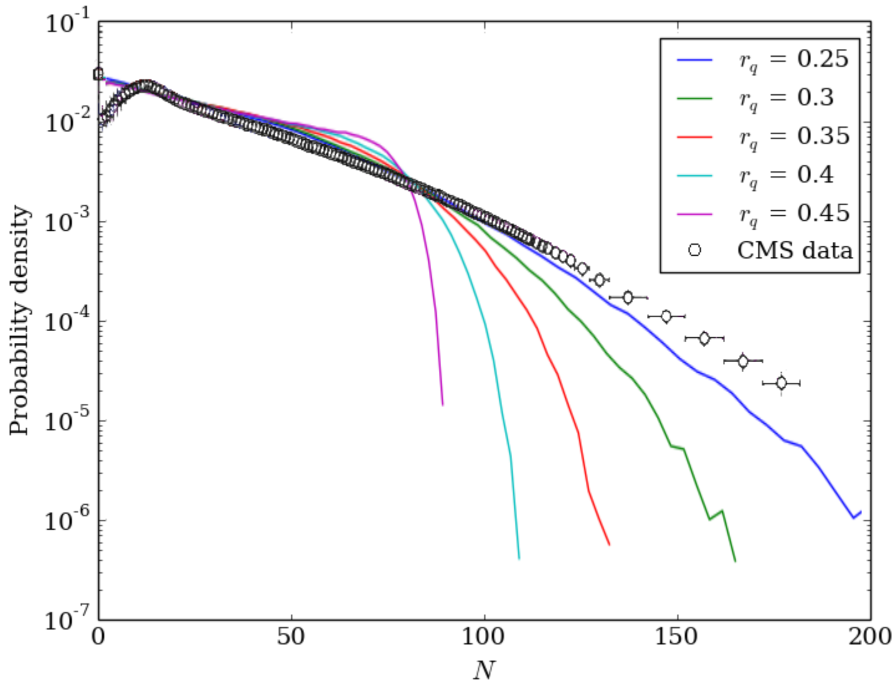

Figure 6.8: Event multiplicity distribution for $\kappa = 0$ compared with [22]

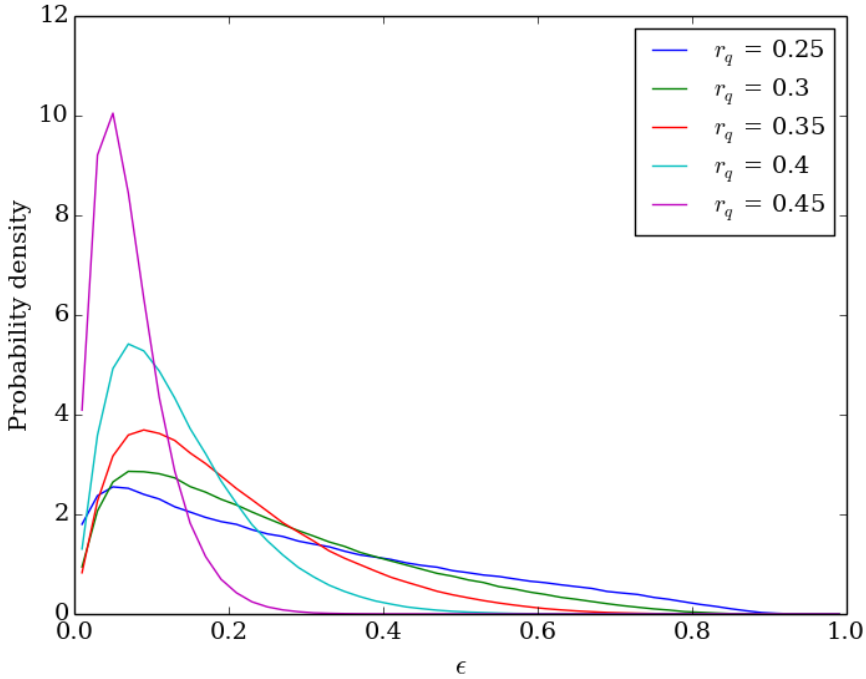

Figure 6.9: Event eccentricity distribution for $\kappa = 0$

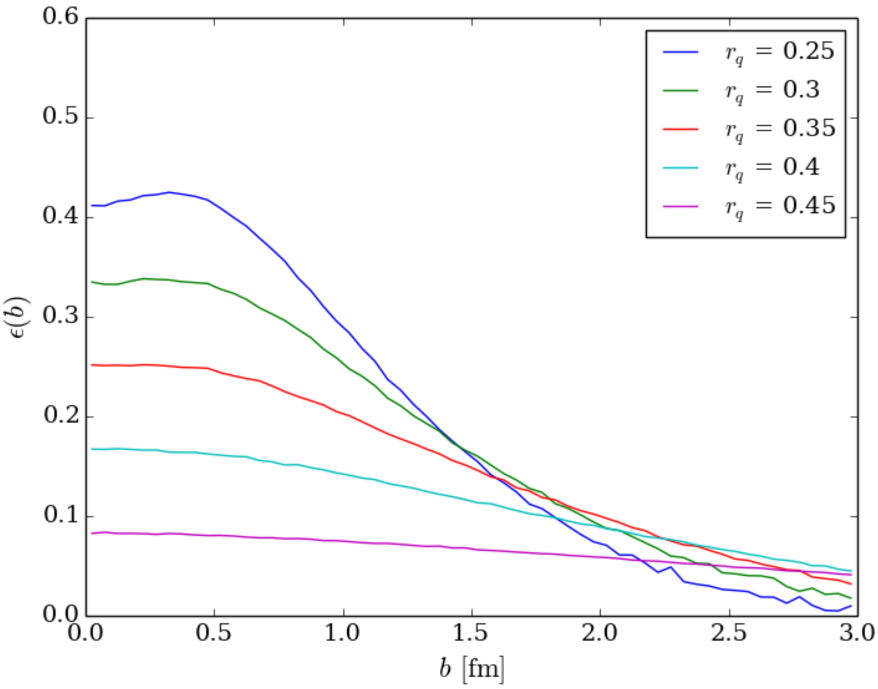

Figure 6.10: Mean eccentricity as a function of b for $\kappa = 0$

Table 6.4: Results for minimum bias and high-multiplicity (HM) events for $\kappa = 0.25$

Input					
Quark radius r_q [fm]	0.25	0.30	0.35	0.40	0.45
Gluon body content κ	0.25	0.25	0.25	0.25	0.25
Effective partonic cross section σ_{gg} [mb]	4.3	4.3	4.3	4.3	4.3
Output					
Effective number of partons N_g	6.7	6.5	6.4	6.2	6.2
Mean number of parton collisions $\langle N_{\text{coll}} \rangle$	2.9	2.7	2.5	2.4	2.4
Produced particles per parton collision α	10.2	11.1	11.8	12.4	12.6
dN/dy per parton collision γ	2.0	2.2	2.3	2.4	2.4
Mean eccentricity $\langle \epsilon \rangle$	0.23	0.20	0.17	0.13	0.15
RMS eccentricity $\sqrt{\langle \epsilon^2 \rangle}$	0.28	0.25	0.20	0.16	0.16
Mean eccentricity in HM events $\langle \epsilon \rangle_{\text{HM}}$	0.24	0.18	0.13	0.09	0.06
RMS eccentricity in HM events $\sqrt{\langle \epsilon^2 \rangle_{\text{HM}}}$	0.28	0.21	0.15	0.10	0.07
Expected elliptic flow $\sqrt{\langle v_2^2 \rangle}$	0.06	0.04	0.03	0.03	0.02
Expected elliptic flow in HM events $\sqrt{\langle v_2^2 \rangle_{\text{HM}}}$	0.06	0.05	0.03	0.02	0.02
Fraction of HM events	0.03	0.03	0.03	0.03	0.06

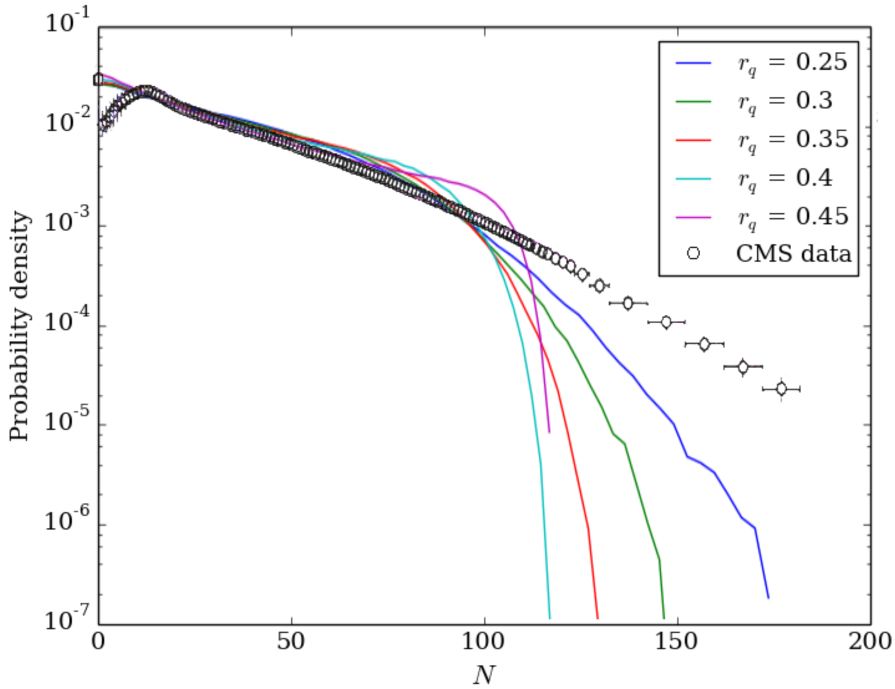

Figure 6.11: Event multiplicity distribution for $\kappa = 0.25$ compared with [22]

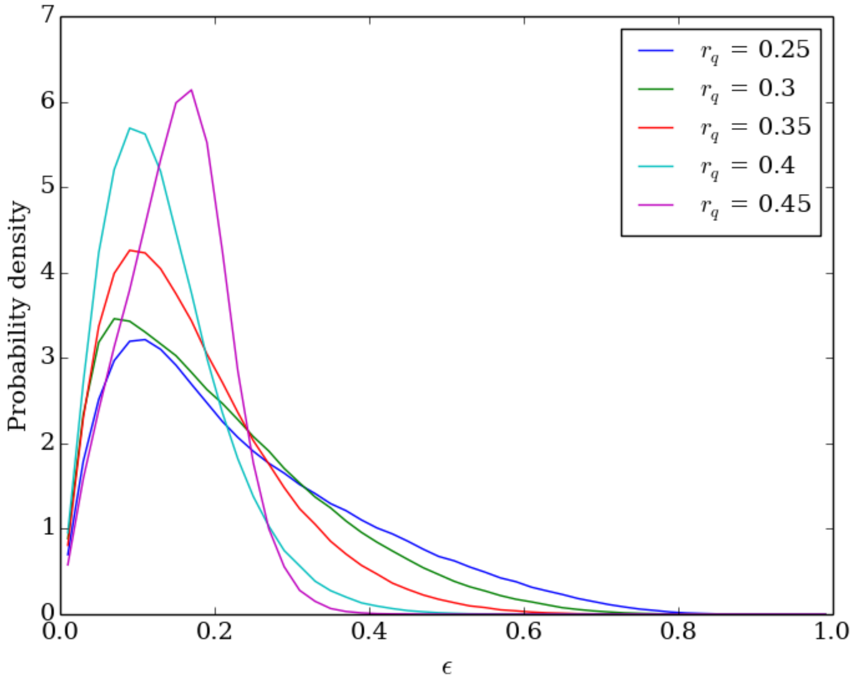

Figure 6.12: Event eccentricity distribution for $\kappa = 0.25$

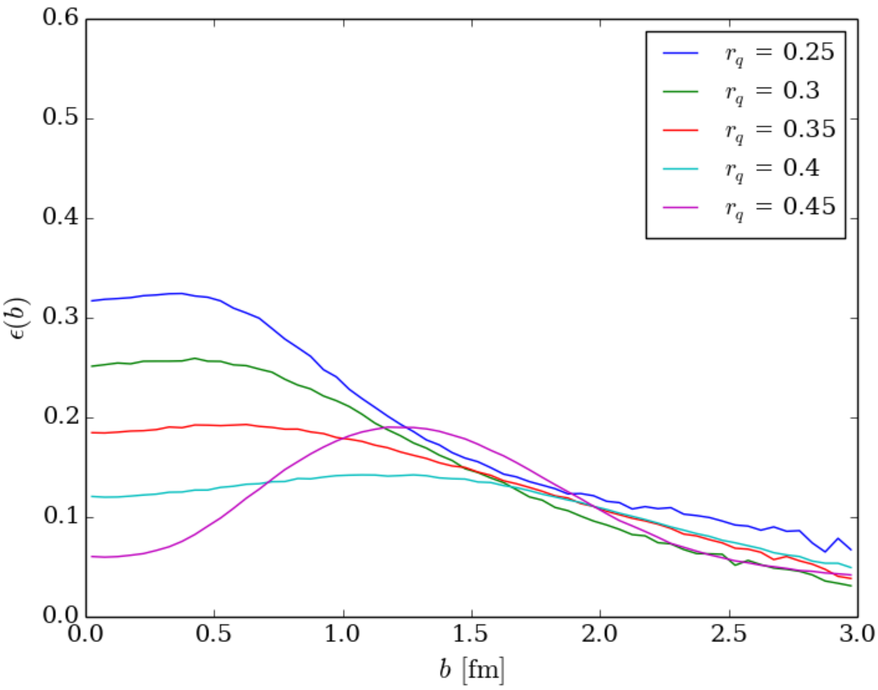

Figure 6.13: Mean eccentricity as a function of b for $\kappa = 0.25$

Table 6.5: Results for minimum bias and high-multiplicity (HM) events for $\kappa = 0.5$

Input					
Quark radius r_q [fm]	0.25	0.30	0.35	0.40	0.45
Gluon body content κ	0.5	0.5	0.5	0.5	0.5
Effective partonic cross section σ_{gg} [mb]	4.3	4.3	4.3	4.3	4.3
Output					
Effective number of partons N_g	6.4	6.6	6.9	7.4	7.6
Mean number of parton collisions $\langle N_{\mathrm{coll}} \rangle$	2.5	2.8	3.1	3.5	3.8
Produced particles per parton collision α	11.8	10.7	9.7	8.5	7.8
dN/dy per parton collision γ	2.3	2.1	1.9	1.6	1.5
Mean eccentricity $\langle \epsilon \rangle$	0.18	0.16	0.14	0.15	0.27
RMS eccentricity $\sqrt{\langle \epsilon^2 \rangle}$	0.22	0.19	0.17	0.17	0.29
Mean eccentricity in HM events $\langle \epsilon \rangle_{\mathrm{HM}}$	0.18	0.13	0.10	0.07	0.06
RMS eccentricity in HM events $\sqrt{\langle \epsilon^2 \rangle_{\mathrm{HM}}}$	0.20	0.15	0.11	0.08	0.07
Expected elliptic flow $\sqrt{\langle v_2^2 \rangle}$	0.04	0.03	0.03	0.02	0.03
Expected elliptic flow in HM events $\sqrt{\langle v_2^2 \rangle_{\mathrm{HM}}}$	0.05	0.03	0.03	0.02	0.02
Fraction of HM events	0.03	0.03	0.04	0.07	0.10

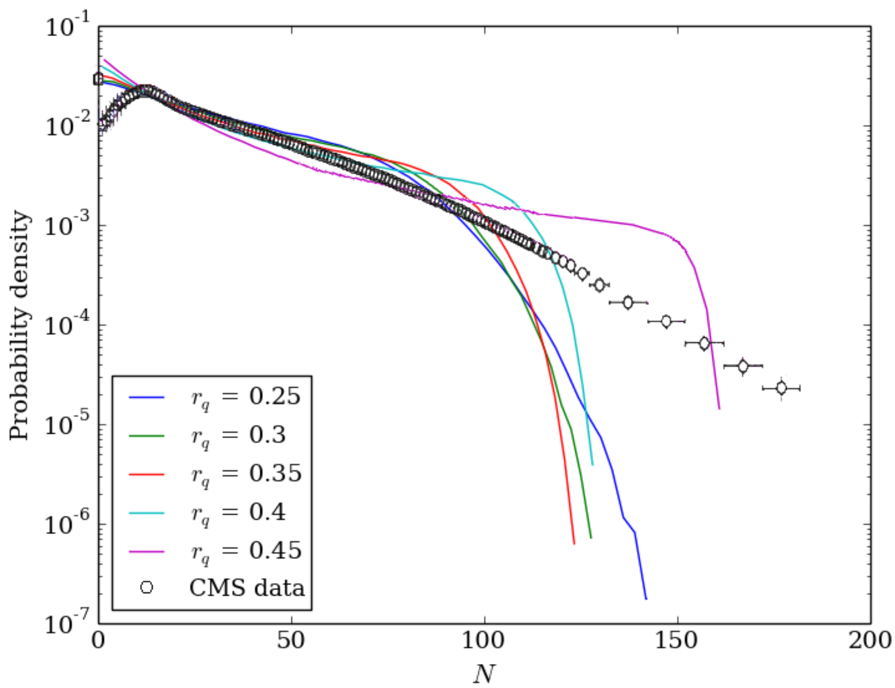

Figure 6.14: Event multiplicity distribution for $\kappa = 0.5$ compared with [22]

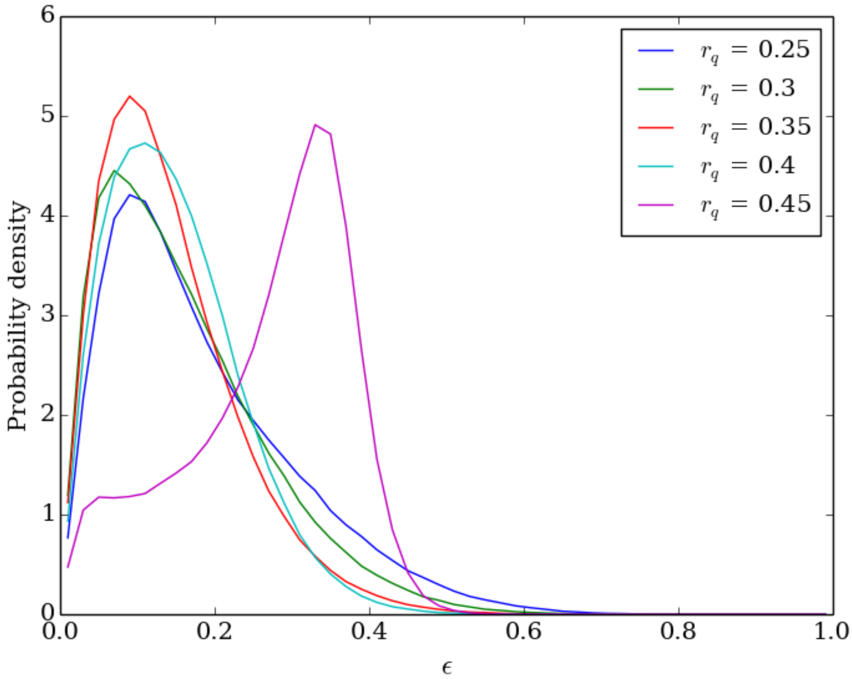

Figure 6.15: Event eccentricity distribution for $\kappa = 0.5$

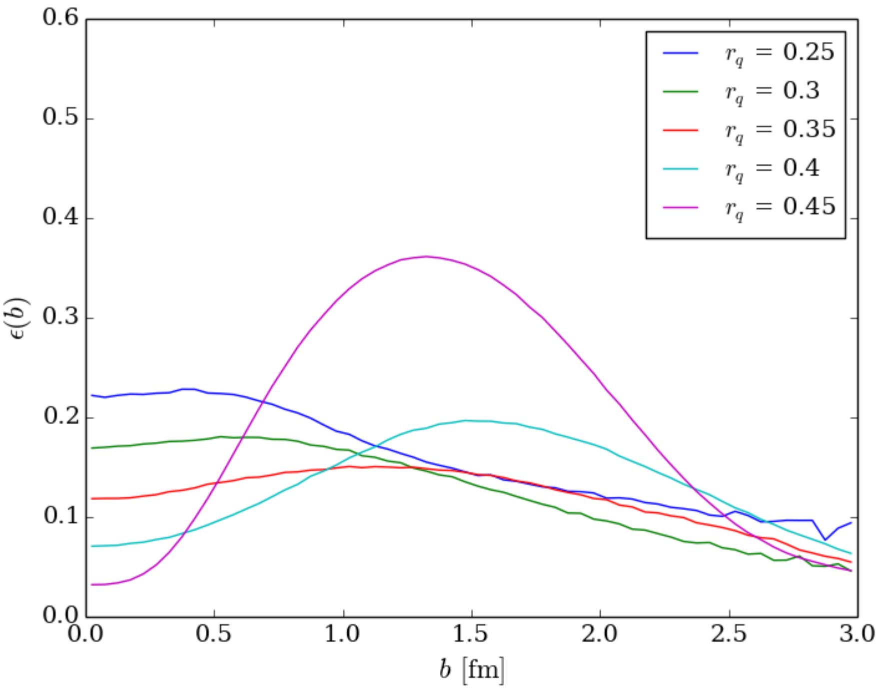

Figure 6.16: Mean eccentricity as a function of b for $\kappa = 0.5$

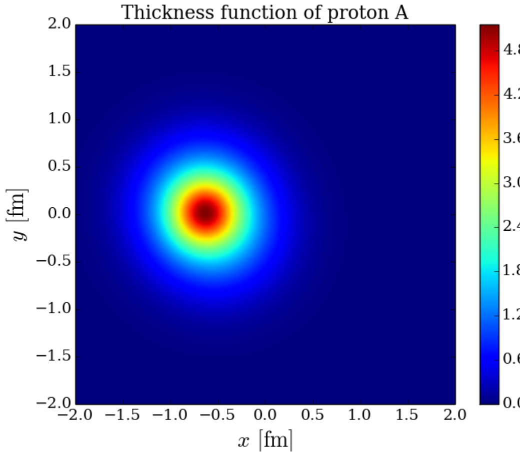

(a)

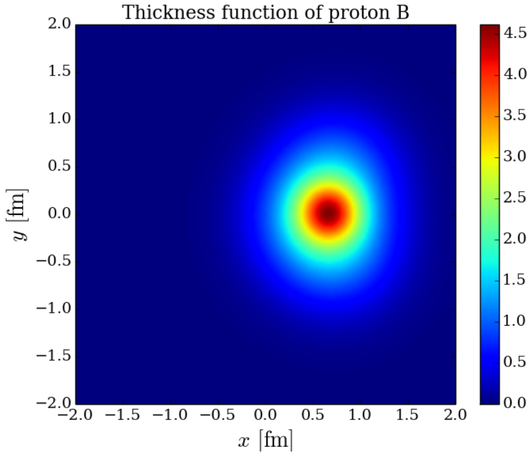

(b)

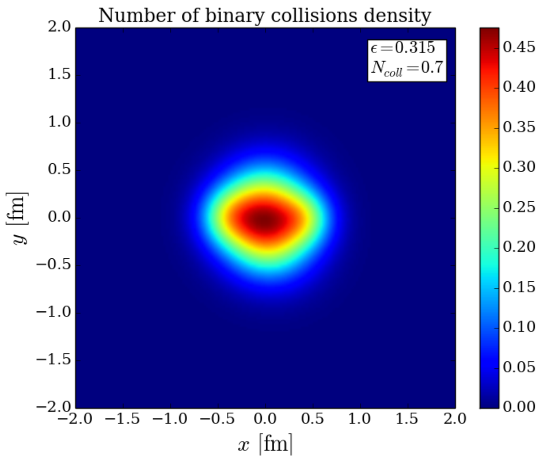

(c)

Figure 6.17: Sample proton densities (a, b) and the collision density (c) for $b = 1.3$ fm, $\kappa = 0.5$, $r_q = 0.45$ fm, $N = 7.6$, $\sigma_{gg} = 4.3$ mb. The total number of partonic collisions and the eccentricity are shown in the picture.

Chapter 7

Discussion

The results of the calculation do not predict an enhancement of elliptic flow in high-multiplicity events. However, it is not contradictory with the observation of the ridge in these events as the ridge height is proportional to the mean multiplicity. What lacks is the better understanding of the non-flow correlations which may obscure the ridge effect in lower multiplicity events.

The mean eccentricity in minimum bias events is generally slightly larger than in high-multiplicity events but the smaller denominator of (3.4) in the latter makes up for this difference. The estimated elliptic flow coefficient for quark radius r_q = (0.25-0.30) fm ($v_2 \approx 0.04$) are in agreement with the possible range of v_2 extracted from the CMS data in [9] (v_2 = 0.04-0.10). If the gluon body content parameter κ is decreased, one can even obtain higher elliptic flow ($v_2 \approx 0.08$) which is still in agreement with the experimental data.

Several authors estimated the elliptic flow coefficient v_2 in pp collisions at $\sqrt{s} = 14$ TeV [24, 25, 26, 27, 28, 29]. Various proton parametrization without fluctuating variables were analyzed in [26] leading to v_2 in range 0.01-0.1. In [28] a simple model of proton made of randomly located Gaussian 'hot spots' were considered implying higher v_2. These results are similar to the prediction of the thesis. It will be probably very difficult to distinguish between these models only by focusing on the ridge effect. Another possible test of the models may be offered e.g. by the attempt to interpret the femtoscopy data on pp collisions [30, 31].

What can be learnt about proton structure is that in order to explain broad multiplicity distribution in pp collisions and initial spatial anisotropies fluctuations some proton's internal degrees of freedom are needed. The positions of 3 effective quarks assumed their role in this thesis. Under the assumptions presented, data on elliptic flow and multiplicity distributions at $\sqrt{s} = 7$ TeV favor effective quark radius of half proton radius. The necessity of central gluon body for describing data is ambiguous as it decreases the effects of configurations' fluctuations. Moreover, it is the source of artificial eccentricities at mid-central collisions. Probably a better parametrization for the gluon medium in proton, taking into account actual quark positions, should be proposed.

Another type of proton's internal structure was investigated in [10]. In that model a proton is made of a quark and a diquark (two closely bound quarks) connected by a flux tube. Two cylinder-like structures like these can have different orientations with respect to each other when they collide. The authors postulated that high-multiplicity events correspond to collisions in which the tubes are perpendicular to direction of the movement and parallel to each other. The area of the interaction is then extremely eccentric. Consequently, the events characterized by the largest overlap of protons are the ones producing the largest elliptic flow. The effective quark model presented in the thesis lacks this kind of an easy to grasp correlation between multiplicity and eccentricity. It would be interesting to parametrize the proton density in the flux tube model and perform the calculations to verify the intuitions.

The reasoning presented here is founded on many simplifications. It is by no means certain that it can explain the physics of *pp* collisions. However, the author hopes that this ideas can serve as a starting point for further more realistic searches of possible footprint of proton's internal structure in the ridge effect.

Acknowledgement

I would like to express my sincere gratitude to Stanisław Głazek for being a demanding though always willing to help advisor.

I am grateful to Piotr Bożek, Stanley J. Brodsky, Paweł Danielewicz, Adam Kisiel and Jean-Yves Ollitrault for fruitful discussions.

My special thanks go to my parents without whose support this thesis could not exist.

Bibliography

[1] V. Khachatryan *et al.* [CMS Collaboration]: Observation of Long-Range, Near-Side Angular Correlations in Proton-Proton Collisions at the LHC *J. High Energy Phys.* **1009**, 091 (2010)

[2] S. Chatrchyan *et al.* [CMS Collaboration]: Observation of Long-Range, Near-Side Angular Correlations in Proton-Lead Collisions at the LHC *Phys. Lett.* **B 718** 795 (2013)

[3] H. Białkowska: The ridge effect from *p-p* to *Pb-Pb* (and back) *Acta Phys. Pol.* **B 43**, 705 (2012)

[4] W. Li: Observation of a ridge correlation structure in high multiplicity proton-proton collisions: a brief review *Mod. Phys. Lett.* **A 27**, 1230018 (2012)

[5] F. Wang: Novel phenomena in particle correlations in relativistic heavy-ion collisions *Prog. Part. Nucl. Phys.* **74**, 35 (2014)

[6] R. Venugopalan: Long range correlations in high multiplicity hadron collisions: building bridges with ridges, arXiv:1312.0113 [hep-ph]

[7] K. Dusling, R. Venugopalan: Azimuthal collimation of long range rapidity correlations by strong color fields in high multiplicity hadron-hadron collisions *Phys. Rev. Lett.* **108**, 262001 (2012)

[8] K. Werner *et al.*: "Ridge" in Proton-Proton Scattering at 7 TeV *Phys. Rev. Lett.* **106**, 122004 (2011)

[9] J. Bożek: Elliptic flow in proton-proton collisions at $\sqrt{s} = 7$ TeV *Eur. Phys. J. C* **71**, 1530 (2011)

[10] J. D. Bjorken, S. J. Brodsky, A. S. Goldhaber: Possible multiparticle ridge-like correlations in very high multiplicity proton-proton collisions, arXiv:1308.1435 [hep-ph]

[11] R. Snellings: Elliptic flow: a brief review *New J. Phys.*, **13**, 055008 (2011)

[12] H. J. Drescher, A. Dumitru, C. Gombeaud, J. Y. Ollitrault: The centrality dependence of elliptic flow, the hydrodynamic limit, and the viscosity of hot QCD *Phys. Rev. C* **76**, 024905 (2007)

[13] R. J. Glauber in *Lectures in Theoretical Physics* ed. W. E. Brittin and L. G. Dunham, 1-315 (1959)

[14] A. Białas A, M. Błeszyński, W. Czyż: Multiplicity distributions in nucleus-nucleus collisions at high energies *Nucl. Phys.* **B 111**, 461 (1976)

[15] M. L. Miller, K. Reygers, S. J. Sanders, P. Steinberg: Glauber Modelling in High Energy Nuclear Collisions *Ann. Rev. Nucl. Part. Sci.* **57**, 205 (2007)

[16] B. Alver *et al.*: Importance of correlations and fluctuations on the initial source eccentricity in high-energy nucleus-nucleus collisions *Phys. Rev.* **C 77**, 014906 (2008)

[17] S. D. Głazek: Hypothesis of Quark Binding by Condensation of Gluons in Hadrons *Few-Body Syst* **52**, 367 (2012)

[18] G. Altarelli, N. Cabibbo, L. Maiani, R. Petronzio: The nucleon as a bound state of three quarks and deep inelastic phenomena *Nucl. Phys.* **B 69** 531 (1974)

[19] L. Hove and S. Pokorski: High-energy hadron-hadron collisions and internal hadron structure *Nucl. Phys.* **B 86** 243 (1975)

[20] R. C. Hwa: Evidence for valence-quark clusters in nucleon structure functions *Phys. Rev.* **D** 22, 759 (1980).

[21] S. Chatrchyan *et al.* [CMS Collaboration]: Measurement of the inelastic proton–proton cross section at $\sqrt{s} = 7$ TeV *Phys. Lett.* **B 722**, 5 (2013)

[22] V. Khachatryan *et al.* [CMS Collaboration]: Charged particle multiplicities in *pp* interactions at $\sqrt{s} = 0.9$, 2.36 and 7 TeV *J. High Energy Phys.* **1101**, 079 (2011)

[23] V. Khachatryan *et al.* [CMS Collaboration]: Transverse-momentum and pseudorapidity distributions of charged hadrons in *pp* collisions at $\sqrt{s} = 7$ TeV *Phys. Rev. Lett.* **105**, 022002 (2010)

[24] M. Luzum, P. Romatschke: Viscous hydrodynamic predictions for nuclear collisions at the LHC *Phys. Rev. Lett.* **103**, 262302 (2009)

[25] S. K. Prasad, V. Roy, S. Chattopadhyay, A. K. Chaudhuri: Elliptic flow (v_2) in pp collisions at energies available at the CERN Large Hadron Collider: A hydrodynamical approach *Phys. Rev.* **C 82**, 024909 (2010)

[26] D. d'Enterria, G. Kh. Eyyubova, V. L. Korotkikh, I. P. Lokhtin, S. V. Petrushanko, L. I. Sarycheva, A. M. Snigirev: Estimates of hadron azimuthal anisotropy from multiparton interactions in proton-proton collisions at $\sqrt{s} = 14$ TeV *Eur. Phys. J. C* **66**, 173 (2010)

[27] P. Bożek: Observation of the collective flow in proton-proton collisions *Acta Phys. Polon.* **B 41**, 837 (2010)

[28] J. Casalderrey-Solana, U. A. Wiedemann: Eccentricity fluctuations make flow measurable in high multiplicity p-p collisions *Phys. Rev. Lett.* **104**, 102301 (2010)

[29] E. Avsar, Ch. Flensburg, Y. Hatta, J.-Y. Ollitrault, T. Ueda: Eccentricity and elliptic flow in proton-proton collisions from parton evolution *Phys.Lett.* **B 702**, 394 (2011)

[30] A. Kisiel: Signatures of collective flow in high multiplicity pp collisions *Phys. Rev.* **C 84**, 044913 (2011)

[31] K. Aamodt *et al.* [ALICE Collaboration]: Femtoscopy of *pp* collisions at $\sqrt{s} = 0.9$ and 7 TeV at the LHC with two-pion Bose-Einstein correlations *Phys. Rev.* **D 84**, 112004 (2011)

[32] J. Beringer *et al.* [Particle Data Group], *Phys. Rev.* **D 86**, 010001 (2012), Section 45

[33] W. Florkowski: Phenomenology of Ultra-Relativistic Heavy-Ion Collisions *World Scientific* (2010)